Journal of Membrane Science 337 (2009) 136–144

Contents lists available at ScienceDirect

Journal of Membrane Science

journal homepage: www.elsevier.com/locate/memsci

CFD modeling of a transient hollow fiber ultrafiltration system for protein concentration

Bernard Marcos[a,*], Christine Moresoli[b], Jana Skorepova[b], Brandi Vaughan[b]

[a] Département de génie chimique, Université de Sherbrooke, Sherbrooke, Canada J1K 2R1
[b] Chemical Engineering Department, University of Waterloo, Waterloo, Canada N2L 3G1

ARTICLE INFO

Article history:
Received 18 November 2008
Received in revised form 21 March 2009
Accepted 24 March 2009
Available online 1 April 2009

Keywords:
Computational fluid dynamics
Modeling
Hollow fibre
Ultrafiltration
Fouling
Soy proteins

ABSTRACT

A transient model based on the finite element method (CFD Comsol) to simulate numerically the flow (momentum equation) and the concentration (diffusion–convection equation) in an ultrafiltration unit is presented. The CFD model was developed by solving the 2D Navier–Stokes equation and the mass conservation equation for transient conditions. A resistance model was used to link the retained protein concentration, the feed and permeate velocity and the pressure at the membrane surface. The ultrafiltration unit consists of a hollow fiber module, a feed tank and a feed pump. In the hollow fiber module, the variable transmembrane pressure, a variable viscosity of the retentate and a polarization layer and a time variable cake occurring on the membrane are considered. Under laminar flow regime, the model allows for the predictions of the velocity fields, the pressure and the concentration along the membrane fiber. The model predictions for the transient permeate flux and the pressure profile in the fiber are compared to experimental data during the concentration of soy protein extracts in a hollow fiber module where total retention of the soy protein is achieved. The comparison shows that the proposed model fits well with the experiments and shows the interest to take into account the variation of resistance and the concentration dependant viscosity flux. The model shows that the transmembrane pressure is an important element on the polarization concentration profile and that a constant transmembrane pressure yields erroneous conclusion on the concentration polarization. The model alleviates some limitations on the polarization modeling avoiding the need to estimate the polarization thickness in the computation of the polarization resistance. The flexibility of the current model is only limited by the ability of the user to accurately define the variations of the properties of the system for industrial applications.

1. Introduction

Membrane technology has received considerable interest over the years for the concentration of soy proteins where proteins are retained by the membrane while the oligosaccharides and minerals are assumed to be removed through the membrane [16]. However, one limitation is the declining permeate flux with time as feed components accumulate on the membrane surface resulting in a polarization layer and possibly a cake formation and pore plugging. It is well known that these phenomena are related by the hydrodynamics of the system contributing to fouling. Accurate predictions of permeate flux and permeate quality are major tasks to design and evaluate membrane processes. To predict accurately the membrane operation and the transient behavior of the permeate flow, it is necessary to model the hydrodynamics and mass transfer phenomena that take place in the bulk solution and at the surface of the membrane.

In the context of membrane separation processes, the simulation approaches may use macroscopic or microscopic models. Most macroscopic models incorporate detailed resistance models such as pore-blocking resistance or cake resistance (Bolton et al. [1], Ho and Zydney [2]) while few microscopic models will include such resistance models. The macroscopic models consist of simplified global mass balance where permeate flux is related to the transmembrane pressure, global membrane resistance, viscosity and other average hydrodynamic parameters. In contrast, the microscopic models use the conservation equations that are solved with the help of numerical scheme either developed by authors (Damak et al. [3], Oxanrago et al. [4], Secchi et al. [5], Sulaiman et al. [6], Geraldes et al. [7], Pellerin et al. [8]), or by available commercial CFD tools (Ahmad et al. [9], Wiley and Fletcher [10], Bessiere et al. [11], Subramani et al. [12]). Broadly speaking, the mass diffusion equation is used but the momentum equation is not always completely solved. For example, Oxanrago et al. [4] used an asymptotic development of the Navier–Stokes equations. Such an approach introduces approximation on the radial velocity and consequently on the permeate flux. It also requires constant viscosity and diffusion although in reality the viscosity may change significantly for protein solutions. Recently,

* Corresponding author. Tel.: +1 819 821 8000x62166.
E-mail address: bernard.marcos@usherbrooke.ca (B. Marcos).

0376-7388/$ – see front matter © 2009 Elsevier B.V. All rights reserved.
doi:10.1016/j.memsci.2009.03.036

Bessiere et al. [11] developed a colloid dead-end filtration model in commercial CFD software taking into account variable diffusivity and viscosity. The microscopic approaches also differ with respect to the boundary conditions. Ahmad et al. [9], Lee et al. [13], Varol et al. [14] assume that the permeate velocity is constant along the fiber but the assumption is not realistic. Geraldes et al. [7] use experimental permeate velocity at different positions as boundary condition, but it is to be noted that the local permeate velocity flow may be quite difficult to measure. Bessiere et al. [11] assume that permeate velocity is variable along the fiber (depending on wall concentration and osmotic pressure) but constant with the time during the transient simulations. The relationship between the local permeate velocity and the different resistances is an important characteristic of the microscopic models. Wiley and Fletcher [10] assumes that the permeate velocity is independent of transmembrane pressure and the global resistance. Some authors consider the polarization layer. However, the definition of the polarization layer thickness is not uniform. Damak et al. [3] and Pak et al. [15] define the thickness of the polarization layer as the distance from the membrane surface to the position where the relative error between the wall concentration and the bulk concentration was inferior or equal to 10^{-3}. Geraldes et al. [7] define the polarization boundary layer thickness as the distance from the membrane surface at which the solute concentration exceeded by 5% the solute concentration in the bulk flow. Ahmad et al. [9] use the simple film theory to compute the thickness of the gel polarization layer but the film theory requires an estimate of the mass transfer coefficient and overestimates the thickness estimation.

Previous studies do not always include an experimental validation of the model (Damak et al. [3]) or may contain important gaps between the model predictions and the experimental data (Suleiman et al. [6]). The differences may come from the incomplete modeling of the resistance (Suleiman et al. [6]) or from some of the assumptions made, a constant viscosity (Secchi et al. [5]), a constant permeate velocity (Lee et al. [13]). Wiley and Fletcher [10] proved that the model predictions change significantly whether constant properties are assumed or if the properties are assumed to depend on the concentration. An accurate solution of the hydrodynamics and diffusion model is important because it enables the accurate computation of the radial velocity (the axial velocity follows closely the classical parabolic profile), the computation of the pressure related to the viscosity and the computation of the concentration. Due to the coupling of the mass and momentum equations, the CFD approach is relevant for solving such problems. Finally, the permeate flux is the important factor of the filtration process and an accurate prediction of the transient permeate flux should include the different fouling mechanisms. In this paper, we present a CFD modeling study for the analysis of the hydrodynamics and the mass transfer considerations in the bulk and at the membrane surface during the transient operation of the concentration of soy protein extracts by ultrafiltration operated at typical constant TMP conditions for soy protein concentration [29]. The concentration of soy protein extracts by cross-flow hollow fiber ultrafiltration is used to develop the model and to provide model predictions that are compared to experimental data. The experimental data enables the model validation.

2. Experimental

2.1. Experimental set-up

A high shear hollow fiber tangential flow membrane ultrafiltration unit was used (Fig. 1). Soy protein extracts were placed in a 2-L feed tank (1). During the filtration, the retentate was returned to the feed tank which agitated the feed solution resulting in homogenous mixing. A Moyno progressing cavity variable speed pump (2) with a

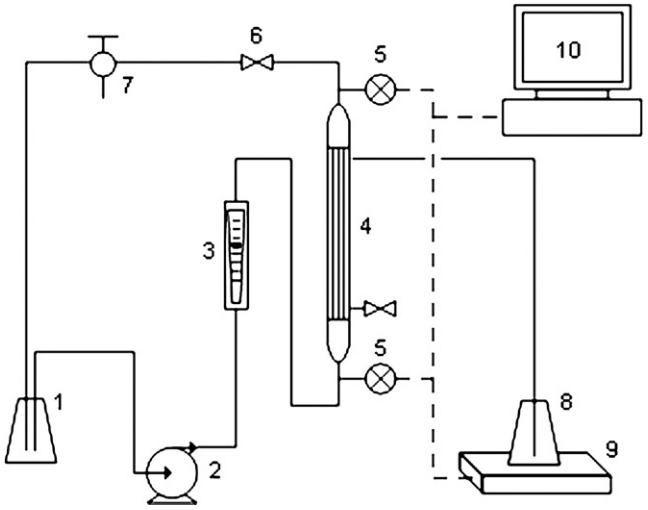

Fig. 1. Schematic diagram of the hollow fiber ultrafiltration experimental system: 1, feed tank; 2, pump; 3, flowmeter; 4, membrane; 5, pressure transducers; 6, pinch valve; 7, sampling valve; 8, permeate container; 9, balance; 10, PC/software.

fluid flow rate of 0–5.68 L/min (0–1.5 GPM) was used to provide high shear pulseless flow to the membrane module. A flow meter (Cole Parmer A-32477-04) was installed on the feed line (3) to measure the flow rate of the feed solution entering the membrane module. A hollow fiber ultrafiltration membrane cartridge (Amersham Biosciences UFP-100-E-4MA) was used (4). The membrane material was polysulphone with a 100-kDa molecular weight cut off. The module was 30 cm in length with 50 fibers of 1 mm inner diameter. The membrane surface area was 420 cm^2. The permeate was collected in a 2-L glass beaker (8) placed on an AdamLab AEP Top loader balance (Cole Parmer A-11700-92) which measured the mass of permeate collected with time enabling the determination of the permeate flux. The capacity of the balance was 2500 g with an accuracy of 0.001 g. Real time data acquisition was achieved via a data acquisition card (10) connected to a PC running Labview®. The data acquisition card was a USB based personal measurement device (Techmatron Instruments PMD-1208LS) which connected directly to the PC where Labview 6.1® was installed. Pressure transducers were placed on the feed (Cole Parmer 0–50 psig A-68075-16), retentate (Cole Parmer 0–50 psig A-68075-16) and permeate (Cole Parmer 0-25 psig A-68075-44) lines to measure the transmembrane pressure.

2.2. Experimental procedure

Soy protein extracts were provided by Agriculture and Agri-Food Canada (St-Hyacinthe, Canada) and produced according to Mondor et al. [17]. The extracts were produced by alkali extraction and had a final pH of 9. For the concentration experiments, the feed solution was prepared by reconstituting a given amount of the powdered extract in a given volume of Nanopure® water. The concentration studies were carried out at 25 °C and at the pH of extracts by drawing off the permeate to achieve a volume concentration ratio (VCR) of 3.5 defined as the ratio between the volume of the feed and the volume of the retentate. A shear rate of 8000 s^{-1} was employed corresponding to a 2.4-L/min feed flowrate (Q_{feed}). The global transmembrane pressure TMP, $TMP = ((P_{in} + P_{out})/2) - P_{Permeate}$, was maintained at 27580 Pa (4 psi) or 41370 Pa (6 psi). At the start of the experiment, the feed solution was circulated with the retentate valve completely open. Permeate flux measurements were taken by measuring the time it takes for 1 g of solution to permeate the membrane. Two permeate flux measurements were taken for every 25 g

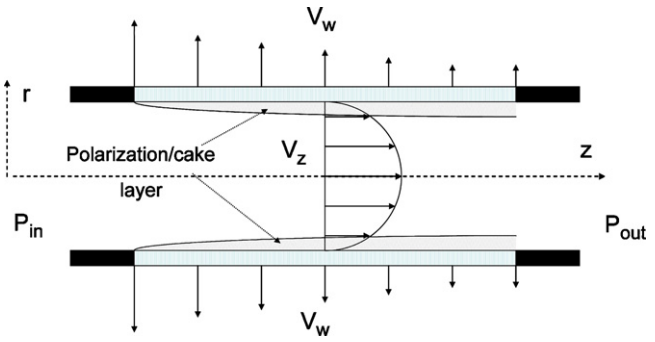

Fig. 2. Simplified representation of the hydrodynamics in the hollow fiber.

of permeate until the appropriate volume of permeate was drawn off to obtain the desired VCR. After each filtration, the membrane was cleaned according to the protocol described by Skorepova and Moresoli [18].

3. Modeling

The system to be modeled consisted of the feed tank (1), the feed pump (2) and the hollow fiber module (4), Fig. 1. The 50-fibers cartridge constitutes the main part of the system. Each fiber consists of a cylinder with radius R and length L surrounded by a porous membrane that acts independently. The diameter (10^{-3} m) and the flow rate ($Q_{feed} < 5.68$ L/min) are small. For the nominal flow rate $Q = 2$ L/min used in the experiments and simulation, the average velocity inside one fiber is $V_{mean} = 4Q/50\pi D^2 = 1.02$ m/s and the maximal Reynolds Number is $DV_{mean}\rho/\mu_w = 1000$. Consequently, the flow is assumed laminar. It is assumed that the polarization layer and the cake do not change significantly the radius of the lumen and this radius is constant during the filtration. Fig. 2 reports a simplified representation of the hydrodynamics inside one fiber. The soy proteins are in low concentration in the bulk so that the solution density is considered constant. However, the effect of the concentration on the viscosity of the solution is considered because viscosity is doubled when the concentration is multiplied by six and the pressure varies strongly with the viscosity (data not shown). The soy protein extract contains approximately 60% proteins, 30% carbohydrates and 10% ash [18]. We assume that the proteins are fully retained when using a 100-kDa membrane and that the carbohydrates and the minerals are free to permeate. The assumption that the minerals are free to permeate is a good initial approximation even though experimental data revealed that there is some retention of the minerals during the concentration operation [18]. The model considers that all the fibers have the same behavior and the permeate flux is the same for all the fibers. Consequently, only one fiber will be modeled.

3.1. Governing equations of hollow fiber

The continuity equation and the Navier–Stokes equation are presented in 2D-cylindrical coordinates for the above assumptions when considering that angular symmetry applies:

$$\frac{\partial v_z}{\partial z} + \frac{1}{r}\frac{\partial r v_r}{\partial r} = 0 \tag{1}$$

$$\rho\left(\frac{\partial v_z}{\partial t} + v_z\frac{\partial v_z}{\partial z} + v_r\frac{\partial v_z}{\partial r}\right) = \frac{1}{r}\frac{\partial}{\partial r}\left(r\mu\frac{\partial v_z}{\partial r}\right) + \frac{\partial}{\partial z}\left(\mu\frac{\partial v_z}{\partial z}\right) - \frac{\partial P}{\partial z} \tag{2}$$

$$\rho\left(\frac{\partial v_r}{\partial t} + v_z\frac{\partial v_r}{\partial z} + v_r\frac{\partial v_r}{\partial r}\right) = \frac{1}{r}\frac{\partial}{\partial r}\left(r\mu\frac{\partial v_r}{\partial r}\right) + \frac{\partial}{\partial z}\left(\mu\frac{\partial v_r}{\partial z}\right) - \frac{\partial P}{\partial r} \tag{3}$$

The equation of conservation is for the protein concentration C, the component retained by the membrane and responsible for the flux decline:

$$\frac{\partial C}{\partial t} + v_z\frac{\partial C}{\partial z} + v_r\frac{\partial C}{\partial r} = \frac{1}{r}\frac{\partial}{\partial r}\left(Dr\frac{\partial C}{\partial r}\right) + \frac{\partial}{\partial z}\left(D\frac{\partial C}{\partial z}\right) \tag{4}$$

3.2. Boundary conditions of a fiber

At the inlet of a fiber, the flow is assumed to be fully developed and a parabolic flow is specified.

$$\text{For } z = 0, \qquad v_z = v_{z,\max}\left(1 - \left(\frac{r}{R}\right)^2\right), \qquad v_r = 0 \tag{5a}$$

At the outlet, the pressure is the atmospheric pressure.

$$\text{For } z = L, \qquad P = P_{atm} \tag{5b}$$

The centerline of the fiber is a symmetry axis:

$$\text{For } r = 0, \qquad \frac{\partial v_z}{\partial r} = 0, \qquad v_r = 0 \tag{5c}$$

At the surface of the membrane fiber, the axial velocity v_z is set to zero (no slip condition) and the radial velocity is set to v_w. v_w is related to the local transmembrane pressure, $\Delta P = P(z,R,t) - P_{Permeate}$ ($P_{Permeate} = P_{atm}$) the viscosity and the different resistances. The expression of v_w is detailed in the following sections.

$$\text{For } r = R, \qquad v_z = 0, \qquad v_r = v_w \tag{5d}$$

At the inlet of the fiber, the protein concentration is taken to be the protein concentration in the feed tank.

$$\text{For } z = 0, \qquad C = C_{feed}(t) \tag{5e}$$

By assuming the total rejection of the proteins, the relationship for the protein concentration at the membrane surface is given as

$$\text{For } r = R, \qquad v_r C - D\frac{\partial C}{\partial r} = 0 \tag{5f}$$

3.3. Governing equations of feed tank

The feed tank is represented as a continuous stirred tank with constant density with:

$$\frac{dV_{feed}}{dt} = Q_{hf} - Q_{feed} \tag{6}$$

$$\frac{dV_{feed}C_{feed}}{dt} = Q_{hf}C_{hf} - Q_{feed}C_{feed} \tag{7}$$

There is no accumulation in the pipe between the feed tank and the hollow fiber module. Consequently, the following mass balance for the proteins provides a relationship between the feed tank and the hollow fiber filtration unit:

$$Q_{hf}C_{hf} = \int_0^R v_z(L, r, t)C(L, r, t)2\pi r\ dr \tag{8}$$

3.4. Physical properties for the solution

The viscosity and the diffusivity of the solution depends on the protein concentration. Several relationships have been proposed to take into account this dependancy. For soy flour extracts, Noordman et al. [19] used an exponential relation supported by a similar

relationship reported previously by Cheryan for the viscosity of soy protein extracts during filtration concentration operation [20]:

$$\mu = \mu_{ref} e^{\alpha(C - C_{ref})} \quad (9)$$

where C is the protein concentration and α is a proportionality constant computed from experimentation [21] with the following numerical values for Eq. (9):

$\mu_{ref} = 2.8 \times 10^{-3}$ Pa s
$\alpha = 0.0095$ L/g
$C_{ref} = 12$ g/L

For the range of concentrations included between 10 g/L and 100 g/L, Malhorta and Couplands [22] obtained similar experimental values for the viscosity of soy protein isolates.

3.5. Initial conditions

At the beginning of the filtration process, the protein concentration in the feed tank and the hollow fiber module is C_{init}. The initial velocity profile is the same as obtained with pure water.

3.6. Permeate flux modeling

The permeate flux decline is induced by the accumulation of the proteins near the membrane surface that are too large to permeate through the membrane. Such an accumulation will induce an increase of the overall membrane resistance. A number of mechanisms may cause the increase of the global membrane resistance, concentration polarization, cake formation and pore blocking. Based on these mechanisms, the global membrane resistance is expressed as follows:

$$R_g = R_m + R_{pol} + R_{cake} + R_{block} \quad (10)$$

with R_m, the clean membrane resistance, R_{pol}, the concentration polarization resistance, R_{cake}, the cake resistance and R_{block}, the blocked pore (internal pore fouling) resistance.

The local permeate velocity at the membrane surface (v_w) will be described by Darcy's law:

$$v_w = \frac{\Delta P}{\mu_0 R_g} = \frac{\Delta P}{\mu_0 (R_m + R_{pol} + R_{cake} + R_{block})} \quad (11)$$

with μ_0 the viscosity of the water.

In the modeling, we distinguish between two transmembrane pressures. The global transmembrane pressure corresponds to $TMP = ((P_{in} + P_{out})/2) - P_{Permeate}$. The TMP was set at 27580 Pa (4 psi) or 42542 Pa (6 psi) during the filtration by adjusting the pinch valve on the retentate line. The local transmembrane pressure (neglecting the osmotic pressure) varies according to the position z, is given as $\Delta P(z,t) = P(z,R,t) - P_{Permeate}$ with $P(z,R,t)$ the pressure of the solution at the inner surface of the membrane (inside the fiber) and $P_{Permeate}$ the pressure (assumed constant) of the permeate (at the outer surface of the fiber). The local transmembrane pressure is calculated by the model for every z position.

A visual analysis of the experimental flux profile with time for the concentration of the soy protein extracts reveals several phases: an initial rapid and significant flux decrease phase; a stabilization phase and a subsequent decrease without stabilization phase. Based on filtration theory for tangential flow ultrafiltration, the first phase may be associated with the formation of polarization layer characterized by a polarization resistance, R_{pol} while the subsequent flux decrease phase may be associated with the formation of a cake layer and pore blocking characterized by R_{cake} and R_{block}. The polarization resistance increases with an apparent time constant τ_{pol} and reaches a limiting value $R_{pol,ss}$ corresponding to the beginning of the pore blocking and the cake formation. The increase of the polarization resistance with time is described with the following differential equation:

$$\tau_{pol} \frac{dR_{pol}}{dt} = (R_{pol,ss} - R_{pol}) R_{pol}(0) = 0 \quad (12)$$

As the polarization is related to the protein concentration at the membrane wall (C_w), the apparent time constant (τ_{pol}) is related to the wall concentration C_w. The apparent time constant varies inversely to the wall concentration. A simple inverse relationship is assumed between τ_{pol} and C_w with proportional constant k_{pol}:

$$\tau_{pol} = \frac{k_{pol}}{C_w} \quad (13)$$

The second term of the Eq. (12) reduces the increase of the polarization resistance when the polarization resistance becomes important. The steady-state polarization resistance is the resistance of the fully developed polarization layer. By representing the dynamics of the polarization layer with Eq. (12), the need to compute explicitly the thickness of the polarization layer is avoided. This is a simplification with respect to several polarization resistance models presented in the literature where the estimation of a specific polarization layer resistance and thickness is required [3,23]. Another characteristic of Eq. (12) is that the polarization resistance changes with the position z because the protein concentration at the membrane surface C_w depends on the position z. Tu et al. [24] present also resistance model based on two ordinary differential equations, but their model uses also an adimensional power law and requires the estimation of the power exponent. As the transmembrane pressure TMP is small, cake compression is unlikely to occur and will not be considered in the following analysis.

Since it is quite difficult to identify the individual contribution of the cake formation and the pore blocking in the last phase of the filtration, the sum $R^*_{block} = R_{block} + R_{cake}$ will be considered in our analysis. As the decrease of the flux is quite important in this phase, the proposed relation for R^*_{block} assumes that the increase of R^*_{block} is linearly proportional to R^*_{block} (complete blocking model). The increase of R^*_{block} is limited by the shear stress induced by main flow described by R_{shear} where R_{shear} is assumed constant in this phase. Consequently, the variation of R^*_{block} will be given by the following differential equation:

$$\tau_{block} \frac{dR^*_{block}}{dt} = R^*_{block} - R_{shear}$$
$$R^*_{block}(t=0) = R^*_{block0} \quad (14)$$

The resistance R^*_{block0} is the initial sum of the resistance when the filtration process begins and corresponds to the resistance of the initial protein adsorption induced by the feed recirculation [2].

3.7. Numerical solution

The mass and momentum equations were solved using the finite element software Comsol (version 3.4). This software has been used previously for filtration modeling by Subramani et al. [12] and Lerch [25]. A two-dimensional, axisymmetric hollow fiber was meshed with mesh generated by the software Comsol, having a very fine mesh near the membrane surface. The automatic meshing on the membrane boundary is controlled by the specified maximum size of element and the growth rate of the elements. This is a classical approach used in finite element method to consider a region with high gradient variation near the membrane. A similar approach was used by Subramani et al. [12], Lerch [25] and Huang and Morrissey [26]. Triangular and quadrilateral elements were tested but no significant differences were observed. The ordinary differential equations describing the resistance dynamics were introduced with the weak formulation on the boundary

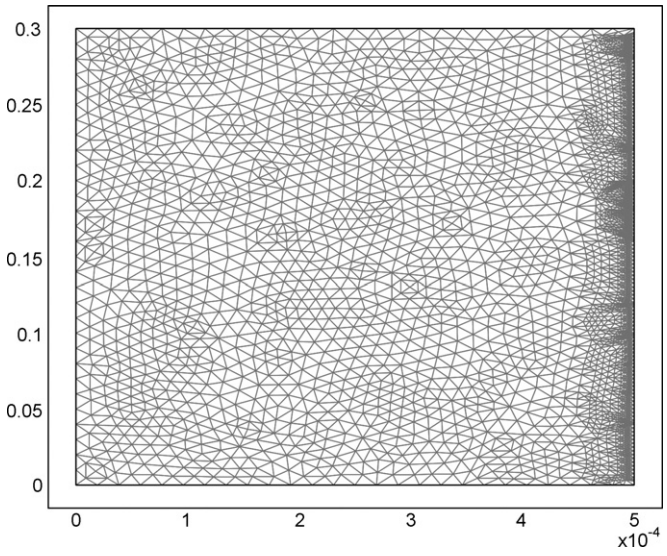

Fig. 3. Mesh used in the numerical simulations.

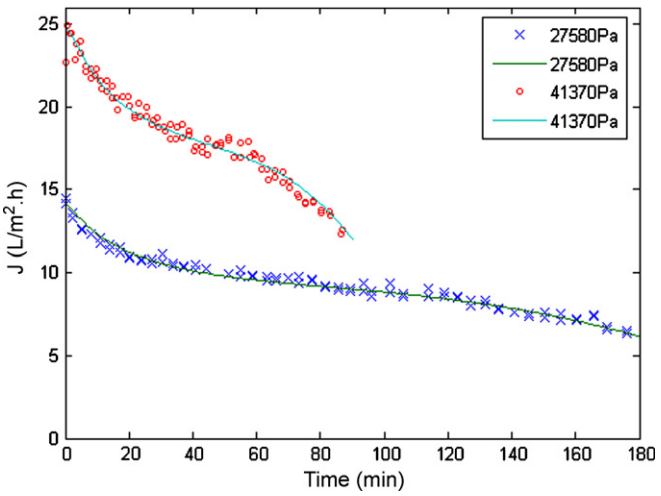

Fig. 4. Permeate flux decline during the concentration of soy protein extracts in a 100-kDa hollow fiber system operated at different pressures, TMP = 41370 Pa (C_{init} = 12 g/L) and TMP = 27580 Pa (C_{init} = 12 g/L).

of the domain. The ordinary differential equations describing the tank dynamics were solved with a Runge Kutta method. The resulting linear equations of the finite element method were solved by using the non-symmetric-pattern multifrontal method and direct LU factorization of the sparse matrix. The method converges when the weighted absolute residual norm is less than 10^{-5}. In order to eliminate the effect of mesh quality and size on the results, different simulations were performed with different mesh resolutions. From these results, the grid illustrated in Fig. 3 containing 3985 elements and 26619 degrees of freedom was chosen because more refined meshing does not change the results of the simulation. The numerical tests were performed on Intel Q9300, 2.5 GHz with 8GB RAM.

4. Results and discussion

The parameters used for the modeling are listed in Table 1. Experiments using pure water as feed solution were used to estimate the membrane resistance R_m. A regression analysis provided the five parameters, τ_{pol}, $R_{pol,ss}$, τ_{block}, R_{shear} and R_{block0}. The range of the initial cake resistance R_{block0} was experimentally estimated as 3.9×10^{12} m^{-1} ± 20% for pH 9 [21].

4.1. Permeate flux dynamics

The permeate flux depends on the local transmembrane pressure and the global resistance according to Eq. (11). Fig. 4 reports the experimental and the predicted permeate flux profile for the feed at TMP = 27580 Pa and TMP = 41370 Pa. With the adjusted five parameters τ_{block}, R_{shear}, τ_{pol}, $R_{pol,ss}$ and R_{block0} the model is able to describe the permeate flux decline during the filtration process. It is important to note that the number of parameters to be estimated is limited and some of them can be roughly evaluated by experiments if R_{block0} is considered as the irreversible component of the global resistance.

The local performance of the filtration can be examined by looking at the permeate velocity (v_w) profile at different times (Fig. 5). This analysis provides details about the local resistance with respect to the time. At the beginning of the filtration operation, the permeate velocity at the membrane surface varies linearly with z, because the permeate velocity follows the behavior of the local transmembrane pressure that also varies linearly with the length z while the protein concentration is constant along the length of the fiber. As the filtration progresses, the predicted permeate velocity decreases and the linear decrease of the predicted permeate velocity with position is reduced. At the end of the filtration (180 min), the predicted permeate velocity is further reduced and is quite low in the last section of the fiber. This indicates that the filtration occurs

Table 1
Parameters used in the model development for the concentration by ultrafiltration of soy protein extracts for a 2.4-L/min feed flowrate (corresponding shear rate (γ) 8000 s^{-1}).

Model parameters	Experiment at TMP = 27,580 Pa	Experiment at TMP = 41,370 Pa
R_m (m^{-1})[a]	2.7×10^{12}	2.5×10^{12}
R_{block0} (m^{-1})	3.30×10^{12}	4.52×10^{12}
τ_{block} (min)	15.5	42.4
R_{shear} (m^{-1})	3.29×10^{12}	4.51×10^{12}
k_{pol} (min^{-1})	1000	900
$R_{pol,ss}$(m^{-1})	2.5×10^{12}	3.5×10^{12}
C_{init} (g/L)[a]	8.9	12
D (m^2/s)	5×10^{-11}	5×10^{-11}

[a] Experimentally determined.

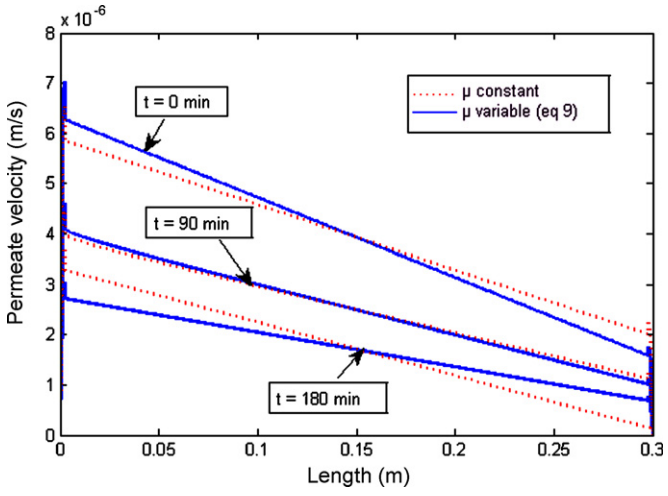

Fig. 5. Predicted permeate velocity at the membrane surface for the concentration of soy protein extracts in a 100-kDa hollow fiber system operated at TMP = 27580 Pa, C_{init} = 12 g/L. with variable viscosity according to Eq. (9) and with constant viscosity.

essentially in the first section of the fiber. At the end of the filtration, the estimated local transmembrane pressure is twice the initial local transmembrane pressure and the increase of this driving force will compensate the increase of the polarization resistance and cake resistance. It is important to consider the contribution of the viscosity to the prediction of the permeate velocity and the pressure profile in the hollow fiber during the filtration process. Different predictions of the permeate velocity, illustrated in Fig. 5, are obtained when assuming a constant viscosity (instead of the concentration dependence viscosity relationship, Eq. (9)). For constant viscosity, the permeate velocity profiles are quite different from those obtained with variable viscosity since the permeate velocity is computed from the local transmembrane pressure, $P(t,R,z) - P_{\text{Permeate}}$ where $P(t,R,z)$ which is obtained by the solution of Navier–Stokes equations containing viscosity. However, the estimates of the average permeate velocity is quite similar whether or not the viscosity was considered variable. Consequently, the permeate flow-rate and the final protein concentration in the feed tank will be similar.

4.2. Resistance dynamics

The evolution with time of the various resistance components constituting the global resistance during the concentration operation is reported in Fig. 6. Mean values were obtained by integrating the local resistance over the membrane surface for the polarization resistance, $\overline{R_{\text{pol}}} = (1/L)\int_0^L R_{\text{pol}}dz$, the pore blocking and the cake deposit resistance, $\overline{R_{block}} = (1/L)\int_0^L R_{block}dz$, their combination, $\overline{R_{\text{pol}}} + \overline{R_{\text{block}}}$ and the global resistance $\overline{R_g}$. Good agreement is observed between the experimental global resistance and the predicted global resistance. The global resistance measured experimentally shows clearly that the variation of the resistance has two phases; the first phase follows a first-order dynamics with steady-state limit and the second phase has an exponential form. The first mechanism is identified to the polarization resistance dynamics. It is an extension to the polarization model proposed by Carrere et al. [27] where a first-order dynamics is used with a time constant independent of the concentration. Such dynamics have been previously associated with incomplete pore blocking model [28]. In the Carrere's formulation, the differential equation has the following form for the mean value of the global resistance over the membrane surface, $\overline{R_g}$:

$$\frac{d\overline{R_g}}{dt} = k_J \Delta P \left(1 - \frac{J^*}{\Delta P}\overline{R_g}\right) \tag{15}$$

Where J^* may be identified to the critical (steady-state value) and k_J is a parameter. Eq. (15) can be rearranged and gives the following equation:

$$\frac{d\overline{R_g}}{dt} = k_J J^* \left(\frac{\Delta P}{J^*} - \overline{R_g}\right) \tag{16}$$

Eq. (16) is used to estimate the steady-state values (corresponding to $\mathrm{d}\,\overline{R_g}/dt = 0$), R^* for the value $\Delta P/J^*$ and a time constant identified to $\tau_{\text{pol}} = (1/(k_J J^*))$. Using this formulation and the experimental data for the concentration of soy protein analyzed in this study, the estimated J^* and R^* presented in Table 2 indicate that the estimates of R^* or J^* may depend on the initial conditions of the filtration and the set transmembrane pressure.

The analysis of the second phase of the filtration with the exponential formulation of the resistance dynamics and the complete pore blocking model [28] represented with the formulation of the classical complete model given as:

$$\frac{d\overline{R_g}}{dt} = k_J J^* \left(\overline{R_g} - \frac{J^*}{\Delta P}\overline{R_g}^2\right) \tag{17}$$

When the second term in Eq. (17) is small, the variation with time of the mean global resistance is proportional to the global resistance and provides an exponential increase. It could be concluded that the second phase of the soy protein filtration corresponds to the beginning of the blocking of the pores rather than cake formation. The presence of pore blockage in the second phase of the filtration agrees with the profile of the flux decline that continues to decline at the end of the filtration.

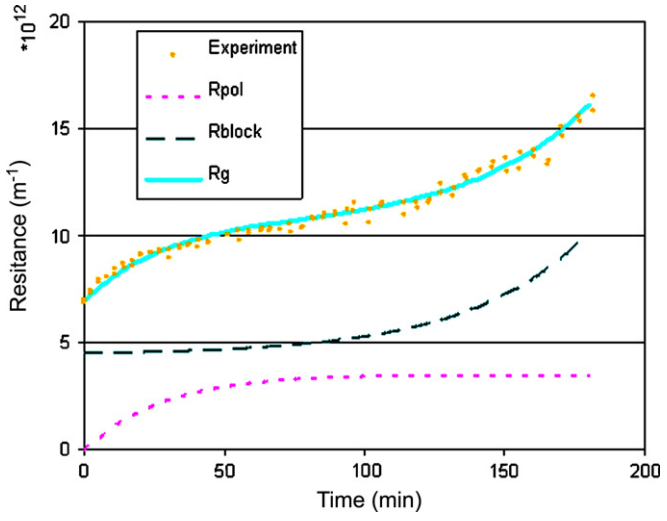

Fig. 6. Evolution with time of the resistances for the concentration of soy protein extracts in a 100-kDa hollow fiber system operated at TMP = 27780 Pa and C_{init} = 12 g/L.

Table 2
Resistance model parameters at steady-state.

TMP (Pa)	J^* (L/m²/h)	R^* (m^{-1})
41,370	18.0	8.4×10^{12}
27,580	9.5	10.7×10^{12}

4.3. Protein concentration profile

Using our model that considers a variable permeate velocity, the protein concentration profile at the membrane surface was estimated for different times as illustrated in Fig. 7. At the end of the filtration (180 min), the maximum protein concentration at the membrane surface is predicted to occur in the first half of the fiber while the minimum protein concentration is predicted to occur at the outlet of the fiber. This profile is different from previous modeling studies where the maximum protein concentration at the membrane surface was reported to occur at the outlet of the fiber [5,9,10]. In these studies, the permeate velocity at the membrane surface (v_w) was assumed constant. When using our model and a constant permeate velocity, $v_w = 10^{-6}$ m/s, instead of the boundary conditions (5a) and (10), the predicted protein concentration at the membrane surface is different as presented in Fig. 7. The predicted protein concentration at the membrane surface reaches the maximum at the exit of the fiber. The more accurate local transmembrane pressure and a computed non-uniform permeate velocity at the membrane surface explains the different predictions presented in Fig. 7. Since it is quite difficult to measure the protein concentration at the membrane surface for a hollow fiber module when using non-destructive techniques, one can obtain a preliminary estimate of the model prediction by consulting the literature. Some experiments with different proteins, BSA, reported polarization concentration with the same order of magnitude as

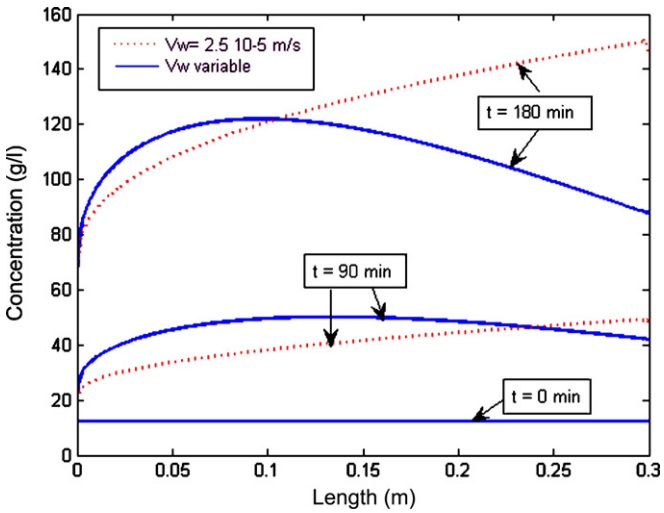

Fig. 7. Protein concentration at the membrane surface for the concentration of soy protein extracts in a 100-kDa hollow fiber system operated at, TMP = 27580 Pa, C_{init} = 12 g/L.

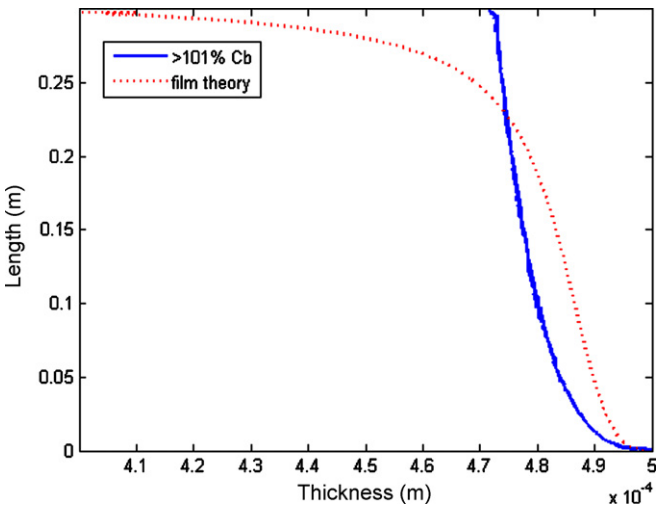

Fig. 9. Predicted polarization layer thickness (>101% C_{bulk}) and film theory at the end of the filtration (t = 180 min) for the concentration of soy protein extracts at TMP = 27580 Pa, C_{init} = 12 g/L.

our predictions [29]. The radial variation of the protein concentration for different times at a fixed fiber length (0.15 m corresponding to 50% of the total fiber length) is illustrated in Fig. 8. The predicted protein concentration remains relatively constant in most of the fiber radial region except for a very thin region near the membrane surface. The concentration dependence of the radial position is controlled by the boundary condition on the membrane wall. In the major part of the fiber, the concentration does not vary with the position and the concentration gradient is zero. With the assumption of total reject, the convective flux is equal to the diffusive flux (in absolute value) on the wall. The wall concentration gradient depends on the large ratio between the diffusivity and the wall velocity and depends on the input concentration. Consequently, the concentration gradient is maximal on the membrane wall and the highest concentration is on the membrane wall.

4.4. Polarization layer

Generally, the analysis of the polarization layer formed near the membrane surface requires the selection of a threshold value at which a polarization layer forms. The selection of this threshold value will affect significantly the intrinsic value of the thickness estimate and consequently the estimate of the resistance of the polarization layer when using the relationship $R_{pol} = R'_{pol}\delta_{pol}$ where R'_{pol} is the specific resistance and δ_{pol} is the thickness of the polarization layer. Typical threshold values reported in the literature are expressed as 1% or 5% of the bulk concentration [3,23]. The thickness of the polarization layer was estimated from the predicted bulk concentration and by defining the limit of the polarization layer as a difference of 1% from the bulk concentration. The estimated thickness of this polarization layer is about 10^{-5} m (2% of inner diameter) as illustrated in Fig. 9. The order of magnitude of the estimate agrees with previous studies [26]. Note that this estimation is based on Eq. (12) and avoids the need to estimate the polarization layer thickness.

An alternative approach to estimate the polarization layer thickness is to use the film theory defined by the following equation:

$$\delta_{pol} = \frac{D}{v_w} \ln\left(\frac{C_w}{C_b}\right) \quad (18)$$

where C_b is the bulk protein concentration (or the centreline concentration). This definition yields the profile illustrated in Fig. 9. Note that the magnitude of the thickness is not very realistic at the end of the filtration. As already mentioned, the film theory amplifies the polarization thickness and may not be a good indicator for the polarization layer.

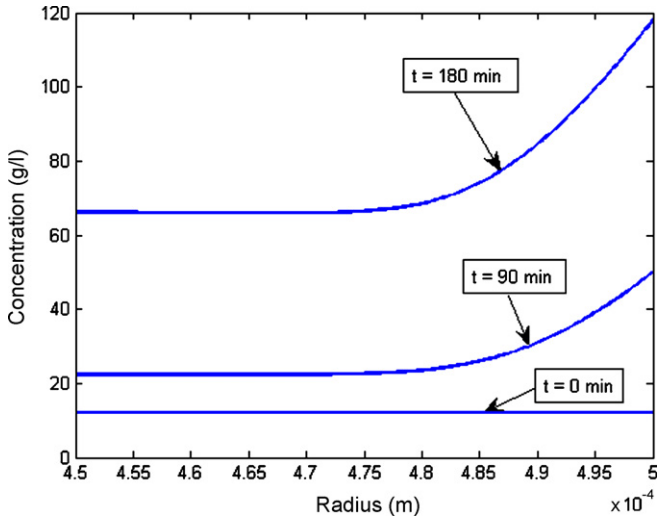

Fig. 8. Predicted protein concentration at z = 0.15 m for the concentration of soy protein extracts in a 100-kDa hollow fiber system operated at TMP = 27580 Pa, C_{init} = 12 g/L.

4.5. Pressure profile

The CFD model developed in this study enables the analysis of the pressure, velocity and protein concentration profile as the filtration proceeds and will be described in this section. The pressure in the hollow fiber at the end of the filtration (t = 180 min) varies linearly with respect to the distance z from the entrance of the fiber and no radial pressure gradient is predicted.

For the hollow fiber, the flow is laminar and the pressure drop along the length of the fiber is well described by Hagen–Poiseuille relationship. In this relation, the pressure gradient (dP/dz) is proportional to the average retentate solution velocity and its viscosity. At any given time, the average axial velocity in the hollow fiber remains practically the same along the fiber because the (radial) permeate velocity (10^{-6} m/s) is very small compared to the retentate (axial) velocity (1 m/s). The predicted velocity profiles show

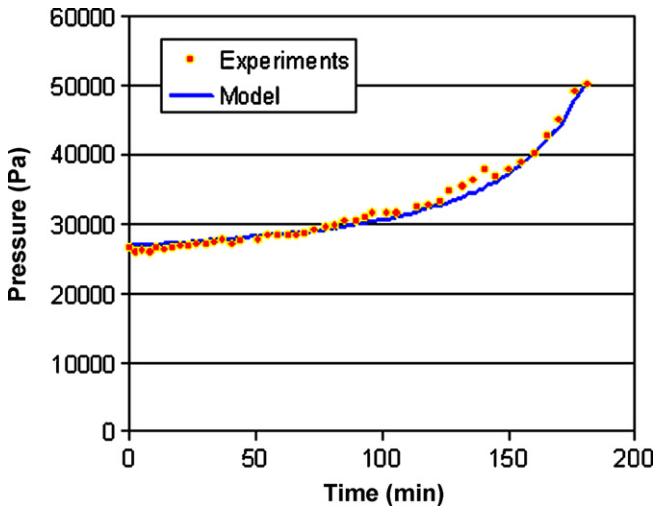

Fig. 10. Pressure difference for the concentration of soy protein extracts at TMP = 27580 Pa and C_{init} = 12 g/L.

that the (axial) velocity is quite independent of the position z and follows the classical parabolic relation with the radius. For the same reason (permeate velocity very small versus axial velocity), at a given time, the protein concentration is quite constant (and equal to the entrance protein concentration) in the hollow fiber, except very close to the membrane surface, where the protein concentration gradient is large.

During the filtration, the protein concentration increases in the retentate and consequently the viscosity of the retentate will also increase. As the pressure difference between the inlet and the outlet of the fiber depends on the viscosity, it is expected that the pressure difference will increase as the filtration proceeds. The evolution with time of the experimental and the predicted pressure difference presented in Fig. 10 shows a very good agreement. One should keep in mind that the fit between the experimental data and the model predictions will depend on the quality of the relationship between the viscosity and the concentration (Eq. (9)) which in our case is a function of the protein concentration. These data show the importance of the variation of the viscosity with protein concentration to describe accurately the evolution with time of the pressure difference.

5. Conclusion

The CFD based model is presented in this study for the prediction of the transient concentration process of soy proteins using a hollow fiber ultrafiltration system. The CFD model was developed by solving the 2D Navier–Stokes equation and the mass conservation equation for transient conditions. The model assumes that all the fibers have the same behavior, the diffusivity is constant and the gravity effect is negligible. As the permeate velocity at the membrane surfaces is generally not known a priori, a resistance model was used to link the retained protein concentration, the feed and permeate velocity and the pressure at the membrane surface. The resistance model considers the formation of a polarization layer and a cake layer. With these assumptions, the model was able to predict the transient permeate velocity and the pressure profiles with a good fit with the experimental data. The model illustrates the importance of the relationship between the viscosity and the protein concentration to predict correctly the transient pressure profiles. The model shows that the transmembrane pressure is an important element on the polarization concentration profile and that a constant transmembrane pressure yields erroneous conclusion on the concentration polarization. The model alleviates some limitations on the polarization modeling avoiding the need to estimate the polarization thickness in the computation of the polarization resistance. While the CFD model developed contains specific equations for the system investigated in this study, the model can be easily modified to encompass any combination of variations in the flux at the membrane surface, rejection, viscosity and diffusivity. The flexibility of the current model is only limited by the ability of the user to accurately define the variations of the properties of the system for industrial applications. Finally, the CFD model succeeded to determine the permeate velocity which is a major indicator of the system performance and the motivation to analyze membrane processes.

Acknowledgements

The authors would like to thank the Natural Sciences and Engineering Research Council of Canada (NSERC) for financial support and Agriculture and Agri-Food Canada, St. Hyacinthe for providing samples for this work.

Nomenclature

Symbols

C	protein concentration (g/L)
C_b	bulk (centerline) protein concentration (g/L)
C_{feed}	feed tank protein concentration (g/L)
C_{hf}	output hollow fiber protein concentration (g/L)
C_{init}	initial protein concentration (g/L)
C_{ref}	reference protein concentration (g/L)
C_w	protein concentration at the membrane surface (g/L)
D	diffusivity (m^2/s)
J	permeate flux ($L/m^2/h$)
J^*	critical (steady-state) flux ($L/m^2/h$)
k_J	resistance constant coefficient
k_{pol}	polarization time constant coefficient (s g/L)
L	fiber length (m)
P	pressure (Pa)
P_{atm}	atmospheric pressure (Pa)
P_{in}	inlet hollow fiber pressure (Pa)
P_{out}	outlet hollow fiber pressure (Pa)
$P_{Permeate}$	permeate pressure (Pa)
Q_{feed}	feed tank volumetric rate (L/min)
Q_{hf}	outlet hollow fiber volumetric rate (L/min)
r	radial coordinate (m)
R	fiber radius (m)
R^*	equivalent steady state resistance (m^{-1})
$R_{blocked}$	fouling resistance (m^{-1})
R_{cake}	cake resistance (m^{-1})
R_{block}	cake and fouling resistance (m^{-1})
R^*_{block}	cake and fouling resistance (m^{-1})
R_{block0}	initial cake and fouling resistance (m^{-1})
R^*_{block0}	initial cake and fouling resistance (m^{-1})
R_g	global resistance (m^{-1})
R_m	clean membrane resistance (m^{-1})
R_{pol}	polarization layer resistance (m^{-1})
$R_{pol,ss}$	steady state polarization layer resistance (m^{-1})
R'_{pol}	specific polarization layer resistance (m^{-2})
R_{shear}	shear rate resistance equivalent (m^{-1})
S	compressibility factor
t	time (min)
TMP	global transmembrane pressure (Pa)
VCR	volume concentration ratio
V_{feed}	feed tank volume (L)

v_r	radial velocity (m/s)
v_w	wall permeate velocity (m/s)
v_z	axial velocity (m/s)
$v_{z,max}$	maximum axial velocity (m/s)
z	axial coordinate (m)

Greek letters

α	viscosity model constant (L/g)
γ	inlet shear rate (m/s)
ΔP	local transmembrane pressure (Pa)
δ	polarization layer thickness (m)
δ_{pol}	polarization resistance model constant (L m/g)
μ	viscosity of protein solution (Pa s)
μ_0	viscosity of water (Pa s)
μ_{ref}	reference viscosity (Pa s)
ρ	specific mass (kg/m^3)
τ_{block}	pore blocking time constant (s^{-1})
τ_{pol}	polarization time constant (s^{-1})

References

[1] G. Bolton, D. LaCasse, R. Kuriyel, Combined models of membrane fouling: development and application to microfiltration and ultrafiltration of biological fluids, J. Membr. Sci. 277 (2006) 75–84.
[2] C.-C. Ho, A.L. Zydney, Transmembrane pressure profiles during constant flux microfiltration of bovine serum albumin, J. Membr. Sci. 209 (2002) 363–377.
[3] K. Damak, A. Ayadi, B. Zeghmatib, P. Schmitz, A new Navier–Stokes and Darcy's law combined model for fluid flow in crossflow filtration tubular membranes, Desalination 161 (2004) 67–77.
[4] L. Oxarango, P. Schmitz, M. Quintard, Laminar flow in channels with wall suction or injection: a new model to study multi-channel filtration systems, Chem. Eng. Sci. 59 (2004) 1039–1051.
[5] A.R. Secchi, K. Wada, I.C. Tessaro, Simulation of an ultrafiltration process of bovine serum albumin in hollow fiber membranes, J. Membr. Sci. 160 (1999) 255–265.
[6] M.Z. Sulaiman, N.M. Sulaiman, B. Abdellah, Prediction of dynamic permeate flux during cross-flow ultrafiltration of polyethylene glycol using concentration polarization-gel layer model, J. Membr. Sci. 189 (2001) 151–165.
[7] V. Geraldes, V. Semiao, M. Norberta de Pinho, The effect on mass transfer of momentum and concentration boundary layers at the entrance region of a slit with a nanofiltration membrane wall, Chem. Eng. Sci. 57 (2002) 735–748.
[8] E. Pellerin, K. Michelitsch, S. Darcovitch, C. Lin, M. Tam, Turbulent transport in membrane module by CFD simulation in two dimensions, J. Membr. Sci. 100 (2) (1995) 139–153.
[9] A.L. Ahmad, K.K. Lau, M.Z. Abu Bakar, S.R.Abd. Shukor, Integrated CFD simulation of concentration polarization in narrow membrane channel, Comput. Chem. Eng. 29 (2005) 2087–2095.
[10] D.E. Wiley, D.F. Fletcher, Techniques for computational fluid dynamics modelling of flow in membrane channels, J. Membr. Sci. 211 (2003) 127–137.
[11] Y. Bessiere, D.F. Fletcher, P. Bacchin, Numerical simulation of colloid dead-end filtration: effect of membrane characteristics and operating conditions on matter accumulation, J. Membr. Sci. 313 (2008) 52–59.
[12] A. Subramani, S. Kim, E.M.V. Hoek, Pressure, flow, and concentration profiles in open and spacer-filled membrane channels, J. Membr. Sci. 277 (2006) 7–17.
[13] Y. Lee, M.M. Clark, A numerical model of steady-state permeate flux during cross-flow ultrafiltration, Desalination 109 (1997) 241–251.
[14] S.S. Varol, N. Yucel, H. Turkoglu, Laminar flow and mass transfer in channels with a porous bottom wall and with fins attached to the top wall, Heat Mass Transf. 36 (2000) 103–108.
[15] A. Pak, T. Mohammadi, S.M. Hosseinalipour, V. Allahdini, CFD modeling of porous membranes, Desalination 222 (2008) 482–488.
[16] N.S. Kumar, M.K. Yea, M. Cheryan, Ultrafiltration of soy protein concentrate: performance and modelling of spiral and tubular polymeric module, J. Membr. Sci. 244 (2004) 235–242.
[17] M. Mondor, D. Ippersiel, F. Larmarche, J.I. Boye, Effect of electro-acidification treatment and ionic environment on soy protein extract particle size distribution and ultrafiltration permeate flux, J. Membr. Sci. 231 (2004) 169–179.
[18] J. Skorepova, C. Moresoli, Carbohydrate and mineral removal during the production of low-phytate soy protein isolate by combined electroacidification and high shear tangential flow ultrafiltration, J. Agric. Food Chem. 55 (2007) 5645–5652.
[19] T.R. Noordman, K. Kooiker, W. Bel, M. Dekker, J.A. Wesselingh, Concentration of aqueous extracts of defatted soy flour by ultrafiltration: effect of suspended particles on the filtration flux, J. Food Eng. 58 (2003) 135–141.
[20] M. Cheryan, Mass transfer characteristics of hollow fiber ultrafiltration of soy protein systems, J. Food Process Eng. (1977) 269–287.
[21] B. Vaughan, High shear cross flow filtration of electroacidified soy protein extracts, thesis, 2005, p. 99.
[22] A. Malhotra, J.N. Coupland, The effect of surfactants on the solubility, zeta potential, and viscosity of soy protein isolates, Food Hydrocolloids 18 (2004) 101–108.
[23] J. Kromkamp, A. Bastiaanse, J. Swarts, G. Brans, R.G.M. van der Sman, R.M. Boom, A suspension flow model for hydrodynamics and concentration polarisation in crossflow microfiltration, J. Membr. Sci. 253 (2005) 67–79.
[24] S.-C. Tu, V. Ravindran, M. Pirbazari, A pore diffusion transport model for forecasting the performance of membrane processes, J. Membr. Sci. 265 (2005) 29–50.
[25] A. Lerch, Fouling layer formation by flocs in inside-out driven capillary ultrafiltration membranes, PhD dissertation, 2008.
[26] L. Huang, M.T. Morrissey, Finite element analysis as a tool for cross flow membrane filter simulation, J. Membr. Sci. 155 (1999) 19–30.
[27] H. Carrere, F. Blaszkowa, H. Roux de Balmann, Modelling the microfiltration of lactic acid fermentation broths and comparison of operating modes, Desalination 145 (2002) 201–206.
[28] R.W. Field, D. Wu, J.A. Howell, B.B. Gupta, Critical flux concept for microfiltration fouling, J. Membr. Sci. 100 (1995) 259–272.
[29] K. Damak, A. Ayadi, B. Zeghmatib, P. Schmitz, Concentration polarisation in tubular membranes—a numerical approach, Desalination 171 (2004) 139–153.